Available online at www.sciencedirect.com
SCIENCE DIRECT®
Talanta 67 (2005) 252–258
Talanta
www.elsevier.com/locate/talanta

Electrochemical study of oxaferrocene cryptands and their complexation with barium and sodium ions

Markus Pagels [a], Andrew W. Meredith [a], Timothy G.J. Jones [a], Richard G. Compton [b], Herbert Plenio [c], Li Jiang [a,*]

[a] *Schlumberger Cambridge Research, High Cross, Madingley Road, Cambridge CB3 0EL, UK*
[b] *Physical and Theoretical Chemistry Laboratory, University of Oxford, South Parks Road, Oxford OX1 3QZ, UK*
[c] *Institut für Anorganische Chemie, TU Darmstadt, Petersenstr. 18, 64287 Darmstadt, Germany*

Received 26 November 2004; received in revised form 11 February 2005; accepted 14 March 2005
Available online 17 May 2005

Abstract

The electrochemical behaviour and cation recognition properties of two oxaferrocene cryptand ligands, 1,1′-[(1,4,10-trioxa-7,13-diazacyclopentadecane-7,13-diyl)diethoxy]-3,3′,4,4′-tetraphenylferrocene and 1,1′-[(1,4,10,13-tetraoxa-7,16-diazacyclooctadecane-7,16-diyl)diethoxy]-3,3′,4,4′-tetraphenylferrocene, have been characterized in acetonitrile in the presence of Ba^{2+} and Na^{+} by cyclic voltammetry, square wave voltammetry and a rotating disc electrode. The changes in the redox signals for the cryptates at varying concentrations of the target cations are used as a direct measure of the electronic coupling between the two units, leading to the conclusion that the cryptate formation process proceeds in multiple stages and the ligand offers several binding sites in the complex.

Keywords: Electrochemistry; Cryptands; Molecular recognition; Binding process

1. Introduction

Molecular recognition systems involving supramolecular host and cation guest(s) are of great interest to the study of complementary binding interactions between molecular species. A prime example of supramolecular ligands that exert significant binding capacity towards alkali and alkaline-earth cations is represented by the cryptand family, developed by Lehn et al. in 1970s [1–5].

The remarkable complexation selectivity of a cryptand is governed primarily by a spherical recognition effect dependent on the size of the closed 3D cavity [1–5]. For instance, cryptand [2.2.1] (4,7,13,16,21-pentaoxa-1,10-diazabicyclo[8.8.5]tricosane) with a cavity radius of 1.1 Å exhibits high specificity towards alkali cations, while cryptand [2.2.2] (4,7,13,16,21,24-hexaoxa-1,10-diazabicyclo[8.8.8]hexacosane) with a cavity radius of 1.4 Å prefers to bind alkaline-earth dications [1]. In order to scrutinize the binding processes, various "reporter groups" whose physical properties change upon binding of a guest ion to the complexation site can be attached to the cryptand. These physical properties can then be monitored, for example, by spectroscopic or electroanalytical means [6]. Ferrocene cryptands are one example of such derivatives that offer a change in the voltammetric signal upon complexing a cation [7]. This property depends on the nature of the inserted cation and can therefore be used in cation sensors or molecular switches. There are in general three types of ferrocene cryptands in which the ferrocene unit and the cryptand part are linked via amide, methyl or ether bonds, respectively.

The first two groups of molecules have been extensively studied with respect to their cation binding capacity and selectivity [8–16]. However, little study has been conducted in detail so far on molecules of the third type with regard to their electrochemistry and complexation reactions [17,18]. Here, we characterize the electrochemical behaviour and cation recognition properties of two such ligands (Scheme 1), namely 1,1′-[(1,4,10-trioxa-7,13-diazacyclopentadecane-7,13-diyl)diethoxy]-3,3′,4,4′-tetra-

* Corresponding author. Tel.: +44 1223 325445; fax: +44 1223 467004.
E-mail address: LJiang@slb.com (L. Jiang).

0039-9140/$ – see front matter © 2005 Elsevier B.V. All rights reserved.
doi:10.1016/j.talanta.2005.03.029

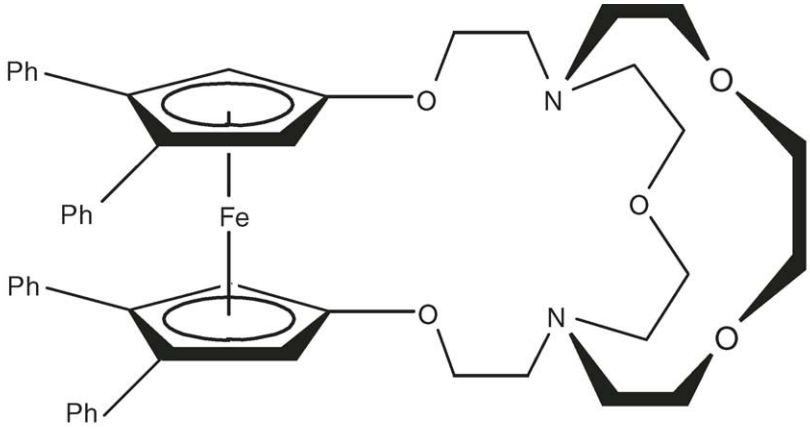

(1) 1,1'-[(1,4,10-trioxa-7,13-diazacyclopentadecane-7,13-diyl)diethoxy]-3,3',4,4'tetraphenylferrocene

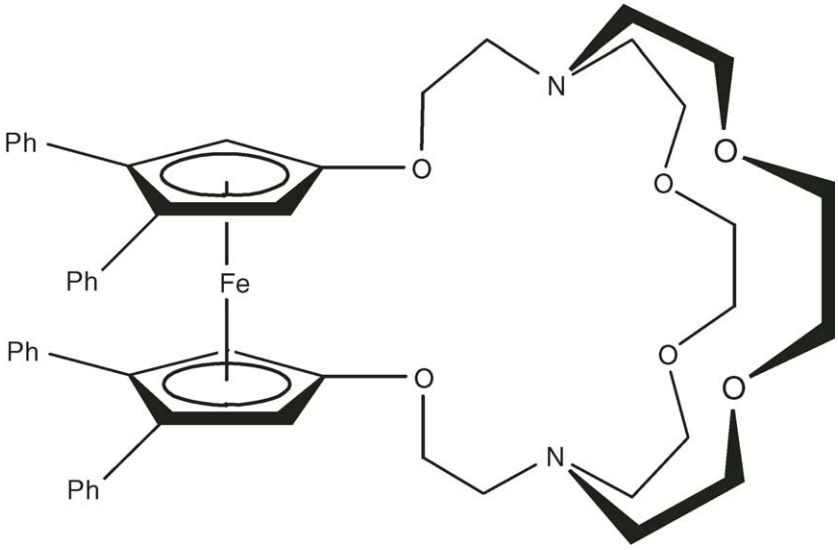

(2) 1,1'-[(1,4,10,13-tetraoxa-7,16-diazacyclooctadecane-7,16-diyl)diethoxy]-3,3',4,4'-tetraphenylferrocene

Scheme 1. Structures of the examined Oxaferrocene cryptands.

phenylferrocene (**1**, analogous to cryptand [2.2.1]) and 1,1′-[(1,4,10,13-tetraoxa-7,16-diazacyclooctadecane-7,16-diyl)diethoxy]-3,3′,4,4′-tetraphenylferrocene (**2**, analogous to cryptand [2.2.2]) in acetonitrile. In particular, we unravel an important aspect of the cation binding process, which, as a function of concentration, can be rationalized by a multi-step mechanism involving several binding sites in the ligand.

2. Experimental

2.1. Electrochemical experiments conditions

A gold disc (diameter 2 mm, area 3.14 mm^2, a roughness factor of 1.44 ± 0.10, was used in the calculation of effective surface area [19]) sealed in a PEEK cylinder was used as the working electrode for cyclic voltammetry and square wave voltammetry, while a larger gold disc (diameter 3 mm, area 7.07 mm^2) was used for rotating disc linear sweep voltammetry. The working electrode was polished with an aqueous aluminium oxide (0.3 μm) slurry and then rinsed thoroughly with deionized water and acetone. Platinum and silver wires were used as counter and quasi-reference electrodes, respectively. Potentials versus the Ag quasi-reference electrode were then rescaled versus Ag/AgCl, which was calibrated with either the ferrocene/ferrocenium redox couple (0.35 V versus Ag/AgCl) or the cobaltocene/cobaltocenium redox couple (−0.96 V versus Ag/AgCl).

For cyclic voltammetry scan rates between 0.01 and 10 V/s were applied. The magnitude of the peak current is proportional to the square root of the potential scan rate up to 10 V/s and over the time span of the experiments, indicating a so-

lution based electron transfer process controlled by the mass diffusion of the reactants. For square wave voltammetry a frequency of $f = 25$ Hz, a step potential of $\Delta E_s = 0.002$ V and an amplitude of $\Delta E_p = 0.02$ V were used. For rotating disk electrode (RDE) experiments rotation rates from 100 to 5000 rpm and a scan rate of $v = 0.02$ V/s were applied.

A computer-controlled electrochemical measurement system with an EcoChemie Autolab PGSTAT30 potentiostat/galvanostat and GPES software was used for electrochemical control and data recording. For the RDE experiments an EcoChemie Autolab RDE with motor controller was used. All electrochemical experiments were carried out in a Faraday cage at ambient temperature and pressure.

Acetonitrile (Aldrich, HPLC grade) and supporting electrolyte tetrabutylammonium hexafluorophosphate (Fluka, electrochemical grade) were used without further purification. The concentration of the supporting electrolyte was 0.1 M.

2.2. Ligand synthesis and characterization

Cryptands **1** and **2** were prepared according to procedures that had been developed by one of the co-authors [17,18].

NMR spectra were recorded at 300 K with a Bruker Avance (^{1}H NMR 200 MHz, ^{13}C NMR 50.3 MHz) spectrometer. ^{1}H NMR spectra were referenced to residual undeuterated solvent, and ^{13}C NMR spectra to the solvent signals: $CDCl_3$ ($\delta(^1H) = 7.26$ ppm, $\delta(^{13}C) = 77.0$ ppm), C_6D_6 ($\delta(^1H) = 7.16$ ppm, $\delta(^{13}C) = 128.0$ ppm), CD_3CN ($\delta(^1H) = 1.93$ ppm, $\delta(^{13}C) = 1.3$ ppm).

2.3. Characterization data for cryptands *1* and *2*

1: 1,1′-[(1,4,10-trioxa-7,13-diazacyclopentadecane-7,13-diyl)diethoxy]-3,3′,4,4′-tetraphenylferrocene: mp = 210 °C, orange colored powder, calculated for $C_{48}H_{52}FeN_2O_5$ (792.8): C 72.72; H 6.61; N 3.53 found: C 72.63; H 6.77; N 3.66.

^{1}H NMR (CD_3CN): δ 2.65–2.69 (m, 8H, NCH_2), 2.87 (t, $J = 6.8$ Hz, 4H, $CpOCH_2CH_2N$), 3.47–3.52 (m, 12H, CH_2O), 4.21 (t, $J = 6.9$ Hz, 4H, $CpOCH_2$), 4.33 (s, 4H, CpH), 6.79–7.00 (m, 20H, PhH).

^{13}C NMR (CDCN): δ 55.9, 57.6, 58.41, 61.9, 70.8, 71.0, 71.4, 71.7, 82.9, 126.9, 127.6, 128.4, 130.8, 137.5.

2: 1,1′-[(1,4,10,13-tetraoxa-7,16-diazacyclooctadecane-7,16-diyl)diethoxy]-3,3′,4,4′-tetraphenylferrocene:
mp = 208 °C, orange colored powder, calculated for $C_{50}H_{56}FeN_2O_6$ (836.8): C 71.76; H 6.74; N 3.35 found: C 71.55; H 6.87; N 3.27.

^{1}H NMR (CD_3CN): δ 2.71–2.77 (m, 8H, NCH_2), 2.94 (t, $J = 7.0$ Hz, 4H, $CpOCH_2CH_2N$), 3.55–3.62 (m, 16H, CH_2O), 4.21 (t, $J = 6.9$ Hz, 4H, $CpOCH_2$), 4.40 (s, 4H, CpH), 6.91–7.09 (m, 20H, PhH).

^{13}C NMR (CDCN): δ 54.9, 56.7, 60.5, 69.8, 70.1, 71.0, 82.0, 125.6, 125.9, 127.3, 129.8, 135.9.

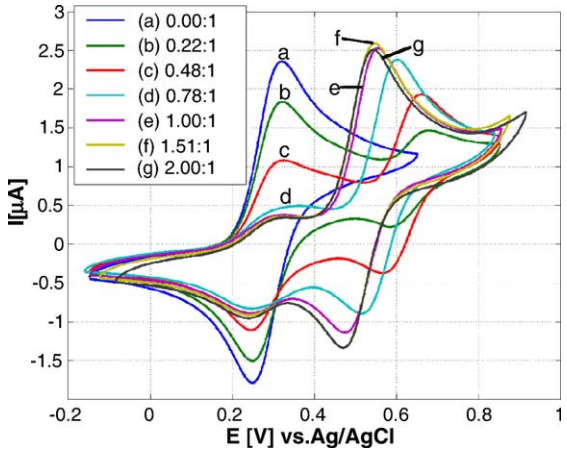

Fig. 1. Cyclic voltammograms of **1** [0.61 mM] with varying concentration ratio $Ba(ClO_4)_2$/**1** in acetonitrile/$TBAPF_6$ (0.1 M), $v = 0.1$ V/s, $T = 20$ °C.

3. Results and discussion

The cyclic voltammograms of **1** and **2** both show a reversible single electron transfer with a half wave potential of $E_{1/2} = 0.285$ V versus Ag/AgCl depicting the oxidation and reduction of the ferrocene moiety (Figs. 1a and 2a). This is in good agreement with corresponding experiments using square wave voltammetry (Fig. 3a).

The diffusion coefficients for **1** and **2** were determined from cyclic voltammetry data at different scan rates as $D_0 = (3.26 \pm 0.58) \times 10^{-6}$ cm^2/s and $D_0 = (3.80 \pm 1.43) \times 10^{-7}$ cm^2/s, respectively. The corresponding heterogeneous electron transfer rate constants are $k_0 = (4.13 \pm 0.61) \times 10^{-3}$ cm/s and $k_0 = (3.27 \pm 0.81) \times 10^{-3}$ cm/s, respectively. These data are well corroborated by experiments with a rotating disc electrode, which gave the corresponding parameters as $D_0 = (5.02 \pm 7.18) \times 10^{-6}$ cm^2/s, $k_0 = (5.12 \pm 3.96) \times 10^{-3}$ cm/s for **1**; and $D_0 = (4.31 \pm 6.30) \times 10^{-6}$ cm^2/s, $k_0 = (3.48 \pm 2.76) \times 10^{-3}$ cm/s for **2**.

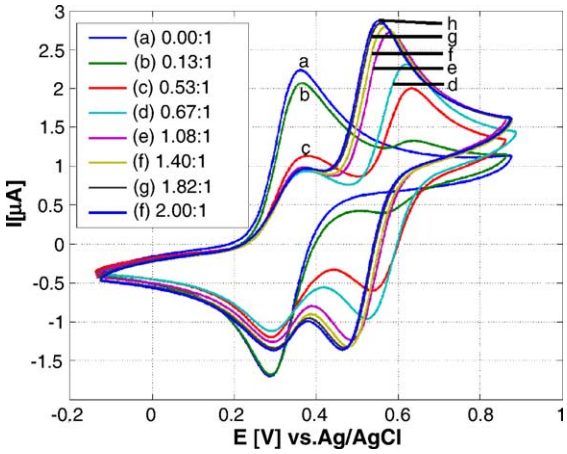

Fig. 2. Cyclic voltammograms of **2** [0.72 mM] with varying concentration ratio of $Ba(ClO_4)_2$/**2** in acetonitrile/$TBAPF_6$ (0.1 M), $v = 0.1$ V/s, $T = 20$ °C.

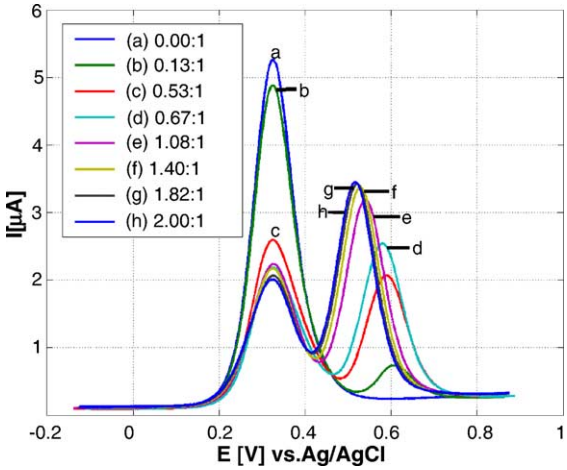

Fig. 3. Square wave voltammograms of **2** [0.72 mM] with varying concentration ratio $Ba(ClO_4)_2$/**2** in acetonitrile/$TBAPF_6$ (0.1 M), $f = 25$ Hz, $\Delta E_s = 0.002$ V, $\Delta E_p = 0.02$ V, $T = 20\,^{\circ}C$.

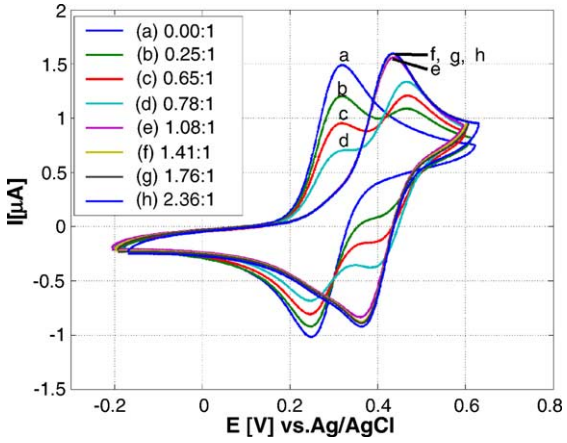

Fig. 4. Cyclic voltammograms of **1** [0.33 mM] with varying concentration ratio $NaClO_4$/**1** in acetonitrile/$TBAPF_6$ (0.1 M), $v = 0.1$ V/s, $T = 20\,^{\circ}C$.

When $Ba(ClO_4)_2$ is added to a solution of **1** in acetonitrile, a second redox pair with a half wave potential at 0.632 V emerges (Fig. 1b). This is caused by the formation of a Ba^{2+}/**1** complex, in which the redox potential of the ferrocene unit is shifted anodically in the presence of additional positive charges of Ba^{2+} at close proximity which makes it less favourable for the ferrocene system to provide an electron. With increasingly higher concentration of Ba^{2+}, the magnitude of the current of the second redox pair grows at the expense of the first couple, indicating a successively higher yield of complexation. Also, surprisingly, the second redox pair shifts cathodically depending on the concentration ratio until reaching a half wave potential of 0.507 V at a Ba^{2+}/**1** ratio of 2/1 (Fig. 1b–g).

Upon addition of an equimolar amount of $NaClO_4$, the redox signal for the Ba^{2+}/**1** complex at 0.632 V completely disappears and is replaced by a new redox pair at around 0.426 V, indicative of the formation of a Na^+/**1** complex. This demonstrates that Ba^{2+} in the complex is readily replaced by Na^+, coinciding with literature that cryptands like **1** preferentially bind Na^+ against Ba^{2+} [1–5].

The presence of $NaClO_4$ in a solution of pure **1** yields a second pair of redox waves with $E_{1/2} = 0.426$ V (Fig. 4a). With successively greater dosage of Na^+, the magnitude of the second redox current enhances at the expense of the first couple, diagnostic of correspondingly higher yields of complexation. Meanwhile, depending on the concentration ratio of cryptand to cation, the redox peak shifts cathodically to a half wave potential of 0.391 V (Fig. 4b–h) as in the case of Ba^{2+}-addition.

Accordingly, addition of $Ba(ClO_4)_2$ to a solution of **2** leads to a second pair of redox waves at a potential of $E_{1/2} = 0.557$ V (Fig. 2b), showing the formation of a Ba^{2+}/**2** complex. With subsequently greater dosage of Ba^{2+}, the magnitude of the second redox current enhances at the expense of the first couple, diagnostic of correspondingly higher yields of complexation. The second pair of waves shifts in the same way, until reaching a half wave potential of 0.456 V at a Ba^{2+}/**2** ratio of 2/1 (Fig. 2c–h).

However, in contrast to the Ba^{2+}/**1** cryptate, the potential of the second redox pair is not affected by the presence of Na^+ or Ca^{2+} at up to 100-fold excess. This demonstrates that the Ba^{2+}/**2** cryptate is a much more stable complex than the Ba^{2+}/**1** cryptate, as cryptand **2** is more favorable towards Ba^{2+} against other mono- and di-valent cations [1–4]. On the other hand, the shift of the second redox wave with increasing metal ion concentration, which can be seen for the above-mentioned cation/cryptand combinations, cannot be detected for the Na^+/**2** complex. The redox signal generated by the coupling of Na^+ and **2** remains constant with a half wave potential of 0.366V across the whole range of concentration ratios (Fig. 5a).

Due to a combination of spherical and electrostatic matching effects, cryptands **1** and **2** exhibit discrete recognition patterns towards the different target cation species over the concentration range, as depicted in Fig. 5. Cryptand **1** displays two distinct yet constant binding domains for Na^+ with

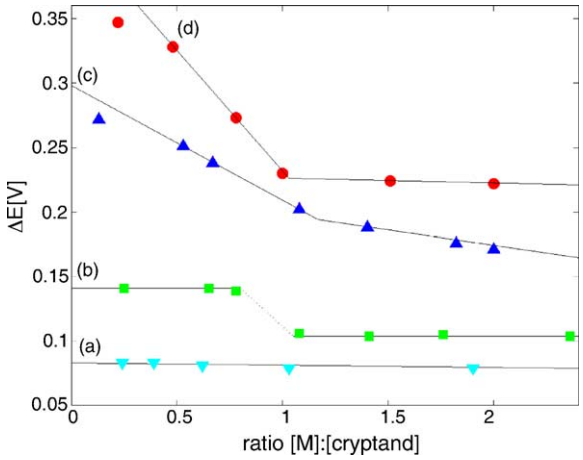

Fig. 5. Over-potential vs. concentration ratio for complexes Na^+/**2** (a), Na^+/**1** (b), Ba^{2+}/**2** (c) and Ba^{2+}/**1** (d).

a turning point around a Na^+/**1** ratio of 1 (Fig. 5b). However, in the case of cryptand **2** the cavity is too large to exert vigorous control on the location of Na^+, evidently leading to a statistical single binding site for Na^+ within the complex across the concentration ratios up to Na^+/**1** = 2 (Fig. 5a).

Nevertheless, cryptand **1** shows two individual binding domains for Ba^{2+} (Fig. 5d). At Ba^{2+}/**1** ratios < 1, there is a gradual decrease in the over-potential at increasingly higher Ba^{2+} dosage, that turns into a constant value at Ba^{2+}/**1** = 1. For cryptand **2**, there are again two distinct binding domains turning into a reduced slope at Ba^{2+}/**2** = 1, yet without reaching an equilibrated value at Ba^{2+}/**2** = 2 (Fig. 5c). All cases show a turning point in slope around a 1/1 ratio, indicating this to be the most probable common composition for these complexes.

It is understood that the magnitude of the over-potential, as a result of the complexation reaction, is proportional to the extent of electrostatic coupling between the ferrocene redox center and the target cation, which is in turn dependent on the distance between the two units. We, therefore, endeavor to use the over-potential as a direct measure of the effectiveness of electrostatic matching, that leads to a rationalization of the aforementioned results based on a concentration dependent, multiple binding site mechanism. Thus the gradual cathodic shift of the second redox wave at successively greater cation dosage indicates a less intensive coupling between M^{n+} and the redox center. This evidently means that M^{n+} is distanced further away from the redox center (Scheme 2). This concentration dependent process leads to the positive charge of the cation being better shielded by the electron donating cryptand arms and, therefore, a thermodynamically more stable configuration with a correspondingly lower over-potential.

It is known that Ba^{2+} is too large to enter the cavity of cryptand **1**. Hence the only location in which the dication can possibly bind to **1** is a side-site (Scheme 2A or B: not identical for **1**). Corresponding to the build up of its concentration, the Ba^{2+} transforms from the initial site into a thermodynamically more stable configuration (Scheme 2D) at Ba^{2+}/**1** = 1. From there onwards the average location of Ba^{2+} remains constant relative to the redox center. On the other hand, when Na^+ encounters **1** initially, it reaches an intermediate status by occupying a side-site (Scheme 2A or B). That is transformed at higher cation concentrations into a thermodynamically more stable configuration in which Na^+ is fully accommodated within the cavity (Scheme 2C) [1–4]. Thus, in the final complex, Na^+ is further displaced from the redox center leading to a lower over-potential.

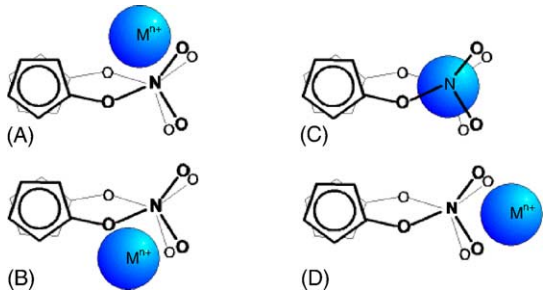

Scheme 2. Possible binding sites of M^{n+} in the M^{n+}/cryptand complex.

As discussed earlier, cryptand **2** does not offer effective binding to Na^+ due to spherical mismatching. However, Ba^{2+} starts its initial interaction with **2** from a side-site (Scheme 2A or B: identical for **2**), which is converted into a thermodynamically more equilibrated site within the cavity (Scheme 2C). This represents a significant insight into the complexing mechanism of the system, which functions in a multiple-step process that is concentration dependent. In a side-site, which is closer to the ferrocenyl oxygen atoms that are the key factor of electronic communication in the system, the charge is distributed among at most four oxygen atoms, including the ferrocenyl oxygen atoms. As such the perturbation to the ferrocene electronic system is more pronounced than when the cation is fully immersed in the cavity, where the positive charge can be distributed among six oxygen atoms and the lone pairs of the two nitrogen atoms. At site D (Scheme 2), the cation imposes little, if any, influence on the electronic system of the ferrocene unit.

The option of forming 2:1 cation/cryptand complexes seems implausible, as in such complexes the cations could attach to the oxaferrocene cryptand only at the outside of the cryptand cavity (Scheme 2A + B, A + D or B + D). As such, the extra charge could not be shielded by the donor atoms. This would lead to a drastic anodic shift of the oxidation potential of the ferrocene unit compared to the redox potential at very low cation concentrations, as the abstraction of an electron would become even more unfavourable than in a 1:1 complex. On the other hand, the formation of 1:2 cation/cryptand complexes at lower concentrations would rather lead to an initially more cathodic redox potential as again the positive charge of the cation would be shielded by two ligands. The redox signals should then shift into anodic direction upon an increase of the metal ion concentration as the shielding becomes less effective for the reason that the total of 1:2 complexes decreases.

In order to make the significance of the potential shift by complex formation more tangible, we introduce a cation binding factor (CBF) analogous to the calculation of the cation binding enhancement previously developed by Gokel et al. for a different host/guest system [20] (Table 1). In the present case, this factor is defined as the ratio of the binding constant for the oxidized ligand–cation interaction (K_{SE}) and the binding constant for the neutral ligand–cation interaction (K_S) with E_f^0 and E_c^0 being the redox potentials for the free ligand and the complex, respectively.

$$\mathrm{CBF} = \frac{K_{SE}}{K_S} = e^{-nF(E_f^0 - E_c^0)/RT}$$

Gokel's cation binding enhancement value was initially used to describe the enhancement of the binding of the cation in the

Table 1
Cation binding factors for complexes of **1** and **2** with Ba^{2+} and Na^{+} at different cation concentration levels

Ba^{2+}/**1**		Na^{+}/**1**		Ba^{2+}/**2**		Na^{+}/**2**	
Concentration ratio	CBF	Concentration ratio	CBF	Concentration ratio	CBF	Concentration ratio	CBF
0.22	930942	0.25	266	0.13	70929	0.24	27
0.48	438626	0.65	266	0.53	34769	0.39	27
0.78	49661	0.78	246	0.67	23398	0.62	25
1.00	9044	1.08	67	1.08	4799	1.03	23
1.51	7131	1.41	62	1.40	3104	1.90	23
2.00	6588	1.76	64	1.82	2261	–	–
–	–	2.36	62	2.00	1930	–	–

complex by the reduction of the ligand. In the present work CBF is used to describe the additional energy that is needed to abstract an electron from the already positively charged complex when the ligand is oxidized. It also represents the extent to which the positive charge of the metal ion is shielded in the complex by the ligand, i.e., "electronic connectivity" between the metal site and the ferrocene redox center.

Clearly noticeable is the difference between the Ba^{2+} and the Na^{+} complexes. This difference, with the Ba^{2+} complexes having much larger cation binding factors than the Na^{+} complexes of ligands **1** and **2**, arises obviously from the difference in charge density of the two ions. As the barium ion has a twofold positive charge, it disturbs the electronic system of the ferrocene unit more than the single positive charge of the sodium ion.

Another difference between the barium and the sodium complexes is the fact, that with increasing concentration ratios the CBF for the Ba^{2+} complexes of **1** and **2** decrease significantly, whereas the CBF for Na^{+}/**1** has two level domains and for Na^{+}/**2** remains constant for all concentration ratios. This means the oxaferrocene cryptands are more susceptible to changes in Ba^{2+} concentration than to changes in the Na^{+} concentration, which is a significant feature for the selectivity of potential sensor applications.

Furthermore, the CBF for Ba^{2+}/**1** has a larger value than the CBF for Ba^{2+}/**2**. This is clearly an indicator that the barium cation is too large to enter the cryptand cavity of ligand **1** and therefore, the charge of the metal ion cannot be shielded as effectively as with ligand **2**. The barium cation in the outside positions (A and B in Scheme 2) is closer to the electronic system of the ferrocene unit and hence the system is more influenced by the positive charge as when the cation is positioned within the cryptand cavity of ligand 2.

4. Conclusion

In summary, we revealed fresh insights concerning the electrochemical behaviour of oxaferrocene cryptands and the binding process of cations to these ligands. Instead of a simple complexation step as expected, our experimental results suggest a far more complex process involving a concentration dependent, multiple-step mechanism with several binding sites. Although the possibility of multiple binding sites was previously raised by one of us [18] and others [16], this is for the first time when definitive experimental evidence is available substantiating the mechanism, which should have profound impact on the further development of the all-important molecular recognition systems and their applications.

Acknowledgement

The authors wish to thank the European Commission for financial support through the Marie Curie Fellowship scheme for M.P. (5th Frame contract number ENK6-GH-02-50522-03).

References

[1] J.M. Lehn, J.P. Sauvage, J. Am. Chem. Soc. 97 (1975) 6700.
[2] J.M. Lehn, Pure Appl. Chem. 50 (1978) 871.
[3] J.M. Lehn, Science 277 (1985) 849.
[4] J.M. Lehn, J.L. Atwood, J.E.D. Davies, D.D. MacNicol, F. Voegtle, Comprehensive Supramolecular Chemistry: Molecular Recognition: Receptors for Molecular Guests, Pergamon Press, Oxford, 1996.
[5] J.H.R. Tucker, Electrochemical Sensors, in: J.L. Atwood, J.W. Steed (Eds.), Encyclopedia of Supramolecular Chemistry, Marcel Dekker, New York, 2004, pp. 505–519.
[6] P.D. Beer, P.A. Gale, G.Z. Chen, J. Chem. Soc., Dalton Trans. (1999) 1897.
[7] P.L. Boulas, M. Gomez-Kaifer, L. Echegoyen, Angew. Chem. Int. Ed. Engl. 37 (1998) 216;
P.L. Boulas, M. Gomez-Kaifer, L. Echegoyen, Angew. Chem. 110 (1998) 226.
[8] C.D. Hall, N.W. Sharpe, I.P. Danks, Y.P. Sang, J. Chem. Soc. Chem. Commun. (1989) 419.
[9] C.D. Hall, I.P. Danks, N.W. Sharpe, J. Organomet. Chem. 390 (1990) 227.
[10] C.D. Hall, J.H.R. Tucker, N.W. Sharpe, Organometallics 10 (1991) 1727.
[11] C.D. Hall, S.Y.F. Chu, J. Organomet. Chem. 498 (1995) 221.
[12] M.C. Grossel, M.R. Goldspink, J.A. Hriljac, S.C. Weston, Organometallics 10 (1991) 851.
[13] H. Plenio, H. El-Desoky, J. Heinze, Chem. Ber. 126 (1993) 2403.
[14] H. Plenio, J. Yang, R. Diodone, J. Heinze, Inorg. Chem. 33 (1994) 4098.

[15] J.C. Medina, T.T. Goodnow, S. Bott, J.L. Atwood, A.E. Kaifer, G.W. Gokel, Chem. Soc. Chem. Commun. (1991) 290.
[16] J.C. Medina, T.T. Goodnow, M.T. Rojas, J.L. Atwood, B.C. Lynn, A.E. Kaifer, G.W. Gokel, J. Am. Chem. Soc. 114 (1992) 10583.
[17] H. Plenio, C. Aberle, Organometallics 16 (1997) 5950.
[18] H. Plenio, C. Aberle, Chem. Eur. J. 7 (2001) 4438.
[19] J.B. Schlenoff, M. Li, H. Ly, J. Am. Chem. Soc. 117 (1995) 12528.
[20] S.R. Miller, D.A. Gutowski, Z. Chen, G.W. Gokel, L. Echegoyen, A.E. Kaifer, Anal. Chem. 60 (1988) 2021.